Saudi Pharmaceutical Journal 32 (2024) 101980

HOSTED BY

ELSEVIER

Contents lists available at ScienceDirect

Saudi Pharmaceutical Journal

journal homepage: www.sciencedirect.com

Original article

Xanthine oxidase inhibition study of isolated secondary metabolites from *Dolichandrone spathacea* (Bignoniaceae): *In vitro* and *in silico* approach

Dang-Khoa Nguyen [a,b], Ta-Wei Liu [a], Su-Jung Hsu [a], Quoc-Dung Tran Huynh [c], Truc-Ly Thi Duong [c], Man-Hsiu Chu [a], Yun-Han Wang [c], Thanh-Hoa Vo [d,1], Ching-Kuo Lee [a,c,*]

[a] School of Pharmacy, College of Pharmacy, Taipei Medical University, Taipei 11031, Taiwan
[b] Faculty of Pharmacy, Ton Duc Thang University, Ho Chi Minh City 700000, Viet Nam
[c] Ph.D. Program in Clinical Drug Development of Herbal Medicine, College of Pharmacy, Taipei Medical University, Taipei 11031, Taiwan
[d] School of Medicine, Vietnam National University Ho Chi Minh City, Ho Chi Minh City 700000, Viet Nam

ARTICLE INFO

Keywords:
Dolichandrone spathacea
Hyperuricemia
Phytochemicals
Xanthine oxidase inhibitors
Enzyme kinetics
Molecular docking

ABSTRACT

Xanthine oxidase (XO) has been widely recognized as a pivotal enzyme in developing hyperuricemia, primarily contributing to the excessive production of uric acid during purine metabolism in the liver. One of the standard treatment approaches involves reducing uric acid levels by inhibiting XO activity. In this study, the leaf extract of *Dolichandrone spathacea*, traditionally used in folk medicine, was found to inhibit XO activity in the ethyl acetate and butanol fractions at a concentration of 100 μg/mL, their values were 78.57 ± 3.85 % (IC_{50} = 55.93 ± 5.73 μg/ml) and 69.43 ± 8.68 % (IC_{50} = 70.17 ± 7.98 μg/ml), respectively. The potential XO inhibitory components were isolated by bioactivity assays and the HR-ESI-MS and NMR spectra system. The main constituents of leaf extracts of *Dolichandrone spathacea*, six compounds, namely *trans*-4-methoxycinnamic acid (**3**), *trans*-3,4-dimethoxycinnamic acid (**4**), *p*-coumaric acid (**5**), martynoside (**6**), 6-O-(*p*-methoxy-*E*-cinnamoyl)-ajugol (**7**), and scolymoside (**17**), were identified as potent XO inhibitors with IC_{50} values ranging from 19.34 ± 1.63 μM to 64.50 ± 0.94 μM. The enzyme kinetics indicated that compounds **3**–**5**, **7**, and **17** displayed competitive inhibition like allopurinol, while compound **6** displayed a mixed-type inhibition. Computational studies corroborated these experimental results, highlighting the interactions between potential metabolites and XO enzyme. The hydrogen bonds played crucial roles in the binding interaction, especially, scolymoside (**17**) forms a hydrogen bond with Mos3004, exhibited the lowest binding energy (−18.3286 kcal/mol) corresponding to the lowest IC_{50} (19.34 ± 1.63 μM). Furthermore, nine compounds were isolated for the first time from this plant. *In conclusion*, *Dolichandrone spathacea* and its constituents possess the potential to modulate the xanthine oxidase enzyme involved in metabolism.

1. Introduction

Xanthine oxidase is the enzyme responsible for the formation of uric acid in the human body. Xanthine oxidase inhibitors, such as allopurinol, steroids, and non-steroidal anti-inflammatory drugs, are used to treat gout by reducing the formation of uric acid or increasing the kidney's ability to eliminate it (Paul and James, 2017, Abdulhafiz et al., 2020). However, prolonged use of synthetic drugs has been associated with severe side effects, prompting investigations into natural compounds as potential alternatives. Natural plant-derived anti-hyperuricemia agents are being studied as alternatives to current therapies due to fewer side effects (Arshad et al., 2018, Choudhary and Mishra, 2019).

Dolichandrone spathacea (D. spathacea) belongs to the Bignoniaceae family and is commonly found growing in the wild along riverbanks and mangrove forests throughout the Asia-Pacific region. The flowers and fruits of *D. spathacea* have been employed to treat conditions such as chlorosis, cholera, diuresis, and haematemesis. The bark has been applied as an antipyretic for asthma, vomiting, inflammation, and diarrhea. The leaves are utilized in treating laxative issues, thrush,

Abbreviations: XO, Xanthine oxidase; EtOAc, Ethyl acetate; BuOH, *n*-Butanol.

* Corresponding author.
E-mail addresses: d301110003@tmu.edu.tw, nguyendangkhoa@tdtu.edu.vn (D.-K. Nguyen), vthoa@medvnu.edu.vn (T.-H. Vo), cklee@tmu.edu.tw (C.-K. Lee).
[1] Co-correspondence author.

https://doi.org/10.1016/j.jsps.2024.101980
Received 6 October 2023; Accepted 30 January 2024
Available online 5 February 2024

asthma, and are being investigated for their potential as antitumor and antiseptic agents. The seeds exhibit disinfectant properties, and the stems are employed in traditional medicine to treat bronchitis (Jackes, 2017, Nguyen et al., 2018, Van Tuan et al., 2018). The phytochemical constituents of this plant were investigated, revealing saponins, flavonoids, phenylethanoid glycosides, iridoids, triterpenoids, steroids, and phenolics constitute the primary bioactive constituents (Nguyen et al., 2016, Thao et al., 2021). Earlier pharmacological studies have shown that it exhibits antioxidant and anti-hyperglycemic effects (Kaewpiboon et al., 2012, Van Tuan et al., 2018) and antimicrobial activity (Saiful et al., 2011, Nguyen et al., 2018). However, the XO-inhibiting components in *D. spathacea* have not been reported and identified previously.

In molecular docking analysis, through the simulation of the ligand's orientation, conformation, and interactions with the protein receptor, docking algorithms can predict potential binding modes of the ligand. Protein-ligand docking simulation is pivotal in computer-aided drug design and gaining insights into biochemical processes. This approach aids in discovering the optimal position for compounds within the protein binding site (Pinzi and Rastelli, 2019, Santos et al., 2019). Previously, we used molecular docking methods to discover xanthine oxidase inhibitors with high binding affinity from alfalfa (Hsu et al., 2021).

Hence, the present study assessed the XO inhibitory potency of the *D. spathacea* extract and its eighteen isolated compounds. Additionally, it investigates the binding interactions between the six bioactive metabolites and the target enzyme by applying molecular docking.

2. Materials and methods

2.1. Plant material

The dried leaves of *D. spathacea* were purchased from the Traditional Medicine Hospital in Ho Chi Minh City, Vietnam, lot number: SL777220, the specification: GLP 236/GNC-QLD; ISO/IEC 17025 VILLAS 486. This material was deposited and researched at the College of Pharmacy, Taipei Medical University, Taiwan.

2.2. General experimental procedures

For isolation and purification of compounds, both normal phase and reverse phase column chromatography with silica gel were used, along with a semi-preparative HPLC. Both normal phase and reverse phase semi-preparative high-performance liquid chromatography (semi-prep-HPLC) were employed, utilizing a Phenomenex® Luna 5 μm Silica 100 Å - semi-preparative LC column 250 × 10 mm and a Purospher® STAR RP-18 end-capped (5 μm) semi-preparative liquid column 250 × 10 mm, respectively. Detection was carried out using an infrared radiation (IR) detector recorded on the Precision Instruments IOTA2 Refractive Index Detector (Marseille, France) and a Hitachi Chromaster 5450 Refractive Index RI Detector (Tokyo, Japan), respectively. The NMR spectrum analysis was conducted using Bruker AV-300 MHz, AV-500 MHz, and AV-600 MHz spectrometers (Bruker, Rheinstetten, Germany). The high-resolution electrospray ionization mass spectrometry (HR-ESI-MS) was recorded on a Q Exactive™ Plus Hybrid Quadrupole-Orbitrap™ Mass (Thermo Fisher Scientific Inc., USA).

2.3. Extraction and isolation

The air-dried leaves of *D. spathacea* (3.0 kg) were soaked in EtOH 95 % (30 L) at room temperature for 7 days, with this process repeated three times in a closed container. The combined ethanolic extract was concentrated under reduced pressure at 45 ℃ to yield a crude extract (400 g). This crude extract was then suspended in water and sequentially partitioned with *n*-hexane, EtOAc, and *n*-BuOH to obtain *n*-hexane, EtOAc, and *n*-BuOH fractions.

The EtOAc fraction (120 g) was chromatographed by a silica gel column and successfully eluted with a gradient mobile phase of n-hexane – EtOAc (v/v) to obtain 10 fractions (A1–10). From the fraction A2, using the semi-preparative HPLC with the normal phase column, obtained compound **1** (20.0 mg) when eluting by the mixture of *n*-hexane – EtOAc (85:15, v/v). Similarly, from the fraction A3, when eluting with the mobile phase of *n*-hexane–EtOAc (80:20, v/v), afforded compounds **2** (7.2 mg); **3** (10.6 mg), **4** (8.3 mg), and **5** (20.8 mg). Additionally, fractions A8 and A10 were purified by reverse-phase semi-preparative HPLC. From fraction A8, using an isocratic system of H_2O–MeOH (25:75, v/v), compound **6** (8.5 mg) was obtained. From fraction A10 with an isocratic system of H_2O–MeOH (45:55, v/v), compound **7** (7.5 mg) was isolated.

The BuOH fraction (70 g) was fractionated by operating the silica gel column chromatography, eluted with a gradient mobile phase of EtOAc – MeOH (v/v) to obtain 5 fractions (B1–5). Fraction B2 was further purified by a particle C_{18} column (7 × 60 cm), eluted with a gradient mixture of H_2O–MeOH (10:1 to 0:1, v/v) to obtain ten fractions (B2.1–2.10). Sub-fractions B2.1, B2.2, B2.3, and B2.5 were chromatographed by reverse phase semi-preparative HPLC with the gradient mobile phase of H_2O–MeOH (v/v). Compound **8** (30.0 mg) and **9** (5.7 mg) were obtained from the sub-fraction B2.1 when using the isocratic system of H_2O–MeOH (85:15, v/v) and H_2O–MeOH (80:20, v/v), respectively. Compound **10** (40.1 mg) was also obtained from sub-fraction B2.2 using the mobile phase of H_2O–MeOH (77:23, v/v). Furthermore, employing the same mobile phase of H_2O–MeOH (70:30, v/v), four compounds, namely, **11** (52 mg), **12** (2.6 mg), **13** (10.1 mg), and **14** (2.6 mg), were purified from sub-fraction B2.3. When eluting sub-fraction B2.5 with the isocratic mobile phase of H_2O–MeOH (65:35), four compounds were obtained: **15** (12.3 mg), **16** (5.8 mg), **17** (4.2 mg), and **18** (8.9 mg). An isolation scheme is presented in Supplementary data Fig. 1S.

2.4. Xanthine oxidase inhibitory assays

The XO inhibition assay was conducted following the protocol described by Hsu et al. (Hsu et al., 2021), with slight adjustments. XO activity was measured in a 96-well microplate (Thermo Scientific™, 96-Well Microtiter™ Microplates, USA) by monitoring uric acid formation at 295 nm. The formation of uric acid results from the reaction between xanthine oxidase and xanthine substrate. The test samples were dissolved in DMSO and then diluted with phosphate buffer. Subsequently, 40 μL of the sample solutions with various concentrations was mixed with 20 μL of 0.1 mM phosphate buffer (pH = 7.5) and 40 μL of enzyme solution (0.005 units/mL in 0.1 mM phosphate buffer, pH = 7.5). The mixture was pre-incubated at 37 °C for 5 min before 100 μL of substrate solution (100 mM xanthine in the same buffer) was added to initiate the reaction. The microplate reader (Thermo Scientific™ Varioskan™ LUX 3020-80587, USA) was used to record the absorbance of the reaction mixture at 295 nm every 30 s for 10 consecutive minutes. Allopurinol was used as the positive control, and the XO inhibitory activity of the test samples was expressed as the percentage inhibition of XO. A blank was prepared similarly, except that XO was not added to the blank solution. The XO inhibitory activity was calculated by the difference in absorbance between samples and control wells. The IC_{50} (half maximum inhibitory concentration) value was calculated using GraphPad Prism 9.5.1 software.

The percentage of XO inhibitory activity was calculated using the following Eq. (1).

$$\text{XO Inhibition } (\%) = (A_O - A_T)/A_O \times 100\% \quad (1)$$

where A_O and A_T represent the absorbances at 295 nm of the blank and the tested samples, respectively.

2.5. Kinetics of xanthine oxidase inhibition

The Lineweaver-Burk plots were analyzed to elucidate the inhibition

mechanisms of the active compounds. This enzyme kinetics investigation assessed the enzymatic reactions in the presence and absence of inhibitors across varying concentrations of xanthine as the substrate (5, 7.5, 10, 12.5, 15, 25, 35, and 50 μM). The initial rates were determined based on the absorbance increase at 295 nm observed between 0.5 and 4 min. The Lineweaver-Burk plots were plotted as Eq. (2).

$$\frac{1}{v} = \frac{K_m}{V_{max}} \frac{1}{[S]} + \frac{1}{V_{max}} \quad (2)$$

where v, $[S]$, and K_m values represent the rate of the enzymatic reaction, the concentration of substrate, and the Michaelis-Menten constant, respectively.

2.6. Molecular docking analysis

The experimental setup and parameter configuration closely followed the methodology previously described by Hsu et al. in 2021. To delve into the binding affinity of the compounds with receptor 1N5X, the CDOCKER Receptor-Ligand Interactions protocol within Discovery Studio software (DS 2021, Accelrys Software Inc., USA) was employed. The crystallographic structure of receptor 1N5X, with its PDB code obtained from the RCSB Protein Data Bank (PDB, https://www.rcsb.org), formed the basis of this study. The compounds were initially represented in 2D structures using ChemBioDraw Ultra 13.3. These 2D representations were converted into the required 3D formats within DS 2021. Following this conversion, an energy minimization step was performed using the conjugate gradient method with a convergence criterion of 0.001 kcal/mol, and it was conducted within the CHARMm force field (Brooks et al., 1983). The resulting energy-minimized structures were subsequently subjected to molecular docking experiments. The preparation of the co-crystallized XO receptor structure (PDB code: 1N5X) involved removing water molecules and adding hydrogen atoms. A dedicated module was used to model the missing loop regions within the prepared protein structure. Additional steps included calculating protein ionization and protonating the protein structure, culminating in a final energy minimization phase optimized for molecular docking. The binding site was defined from PDB site records and the edit binding site module, and the binding site sphere (x: 97.2401, y: 54.6928, z: 37.9714, radius 15) of 1N5X was selected for molecular docking analysis. Afterward, the energy-minimized XO-inhibited compounds were docked into the binding site of 1N5X using the CDOCKER program embedded in DS 2021. The lowest scoring pose for compounds, according to the binding free energy, was selected as the most appropriate pose as potential inhibitors of xanthine oxidoreductase. The ligand-binding free energy for the complex was calculated based on Generalized Born with Molecular Volume (GBMV) (Lee et al., 2003).

2.7. Statistical analysis

GraphPad Prism ed. 9.5.1 (GraphPad Software Inc, CA, USA) was used for data analysis, and data were expressed as mean ± standard deviation (mean ± SD). The inhibitory abilities IC_{50} between the crude extract and fractions were statistically analyzed for differences using one-way ANOVA using Dunnett's Test when the p-values were <0.05 and <0.01.

3. Results

3.1. Determination of the potential XO inhibitory activity of the crude extract, and fractions

The XO inhibitory activity results of *D. spathacea* extract and fractions are shown in Fig. 1. At a concentration of 100 μg/mL, the crude extract exhibited xanthine oxidase (XO) inhibitory activity of 61.43 ± 8.41 %. After further fractionation, the highest activity was observed in

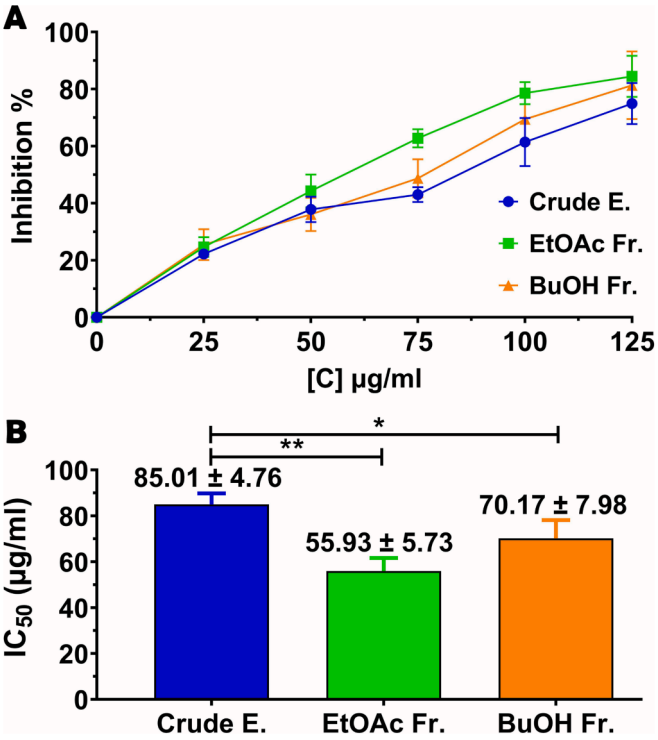

Fig. 1. XO inhibitory activity of crude extract and fractions from *D. spathacea*. (A) Inhibition capability against xanthine oxidase based on concentrations; (B) IC_{50} values of crude extract and fractions. Results are expressed as mean ± SD of three independent experiments. * $p < 0.05$; ** $p < 0.01$ by one-way ANOVA using Dunnett's Test as compared to crude extract.

the EtOAc fraction, followed by the BuOH and hexane fractions, with percentages of 78.57 ± 3.85 %, 69.43 ± 8.68 %, and 27.11 ± 2.50 %, at 100 μg/mL (Fig. 1**A** and Supplementary data Table 2S). It can be seen that the XO inhibitory capability of the hexane fraction is low, and even when the concentration is increased to 200 μg/mL, the inhibition rate is only 32.82 ± 10.13 %; hence we focused on EtOAc and BuOH fraction. In addition, the inhibitory abilities of the EtOAc and BuOH fractions, with IC_{50} values of 55.93 ± 5.73 μg/mL and 70.17 ± 7.98 μg/mL, respectively, are significantly lower than that of the crude extract, which has an IC_{50} value of 85.01 ± 4.76 μg/mL (Fig. 1B). The result indicated that EtOAc and BuOH fractions contain ingredients with xanthine oxidase inhibitory potential.

3.2. Structure identification of the potential xanthine oxidase inhibitory constituents of the EtOAc and BuOH fractions

The crude extract of *D. spathacea* leaves was suspended in distilled water and successfully partitioned with *n*-hexane, ethyl acetate, and *n*-butanol. The EtOAc and BuOH fractions exhibited promising bioactivities and were further purified by column chromatography and semi-preparative HPLC. The structures of all isolated compounds were elucidated based on the 1D and 2D NMR, HRESI-MS, and comparison with reference literature. Nine compounds were obtained from this species, which were previously unreported, including 5α-stigmastane-3,6-dione (**1**) (Zhao et al., 2005); oleanolic acid (**2**) (Onoja and Ndukwe, 2013); martynoside (**6**) (Calis et al., 1984); cistanoside F (**9**) (Kim et al., 2007); 1-(α-L-rhamnosyl(1–6)-*β*-D-glucopyranosyloxy)-3,4,5-trimethoxybenzene (**10**) (Andrianaivoravelona et al., 1999); (+)-lyoniresinol-3α-*O*-*β*-D-glucopyranoside (**11**); (−)-lyoniresinol-3α-*O*-*β*-D-glucopyranoside (**12**); (−)-5′-methoxyisolariciresinol-3α-*O*-*β*-D-glucopyranoside (**13**); (−)-isolariciresinol-3α-*O*-*β*-D-glucopyranoside (**14**) (Wen et al., 2012), and salvionoside B (**18**) (Takeda et al., 1997), along with nine known compounds: *trans*-4-methoxycinnamic acid **(3)** (Bylka, 2004);

trans-3,4-dimethoxycinnamic acid **(4)** (Ralph et al., 2004); *p*-coumaric acid **(5)** (Rho and Yoon, 2017); 6-*O*-(*p*-methoxy-*E*-cinnamoyl)-ajugol **(7)** (Nguyen et al., 2018); ixoside **(8)** (de Santana Aquino et al., 2017); verbascoside **(15)** (Ibrahim Dirar et al., 2019); isoverbascoside **(16)** (Suo et al., 2013); scolymoside (luteolin 7-*O*-rutinoside) **(17)** (Guvenalp et al., 2015), that were previously isolated from this plant. The structures of eighteen compounds isolated from *D. spathacea* are shown in Fig. 2.

The spectroscopic data of the six compounds with potential XO inhibitory activity are shown below; the data for the other compounds of *D. spathacea* are presented in Supplementary data Table 1S and Fig. 2S-54S.

Trans-4-methoxycinnamic acid **(3):** white crystalline powder, HRESI-MS $[M + H]^+$ *m/z* 179.0704, $C_{10}H_{10}O_3$. ^1H NMR (500 MHz, $CDCl_3$) δ_H 7.73 (d, $J = 15.9$ Hz, 1H, H-7), 7.51 (d, $J = 8.8$ Hz, 2H, H-2,6), 6.92 (d, $J = 8.8$ Hz, 2H, H-3,5), 6.32 (d, $J = 16.0$ Hz, 1H, H-8), 3.85 (s, 3H, 3H-OMe) (Bylka, 2004).

Trans-3,4-dimethoxycinnamic acid **(4):** white crystalline powder, HRESI-MS $[M + H]^+$ *m/z* 209.0810, $C_{11}H_{12}O_4$. ^1H NMR (500 MHz, $CDCl_3$) δ_H 7.73 (d, $J = 15.8$ Hz, 1H, H- α), 7.14 (dd, $J = 8.4$, 2.0 Hz, 1H, H-6), 7.08 (d, $J = 2.0$ Hz, 1H, H-2), 6.89 (d, $J = 8.3$ Hz, 1H, H-5), 6.32 (d, $J = 15.9$ Hz, 1H, H- β), 3.93 (s, 6H, 3H-OMe, 3H-OMe). ^{13}C NMR (125 MHz, MeOD) δ_C 171.4 (C- γ), 151.7 (C-4), 149.4 (C-3), 147.2 (C-α), 127.2 (C-1), 123.3 (C-6), 114.7 (C-β), 111.2 (C-5), 109.9 (C-2), 56.2 (C-OMe), 56.1 (C-OMe) (Ralph et al., 2004).

p-Coumaric acid **(5):** white amorphous powder, HRESI-MS $[M + H]^+$ *m/z* 165.0547, $C_9H_8O_3$. ^1H NMR (500 MHz, MeOD) δ_H 7.62 (d, $J = 15.9$ Hz, 1H, H-7), 7.47 (d, $J = 8.7$ Hz, 2H, H-2, 6), 6.82 (d, $J = 8.7$ Hz, 2H, H-3, 5), 6.30 (d, $J = 15.9$ Hz, 1H, H-8). ^{13}C NMR (125 MHz, MeOD) δ_C 171.1 (C-9), 161.2 (C-4), 146.6 (C-7), 131.1 (C-2, 6), 127.3 (C-1), 116.8 (C-3, 5), 115.7 (C-8) (Rho and Yoon, 2017).

Martynoside **(6):** white amorphous powder, HRESI-MS $[M + FA-H]^-$

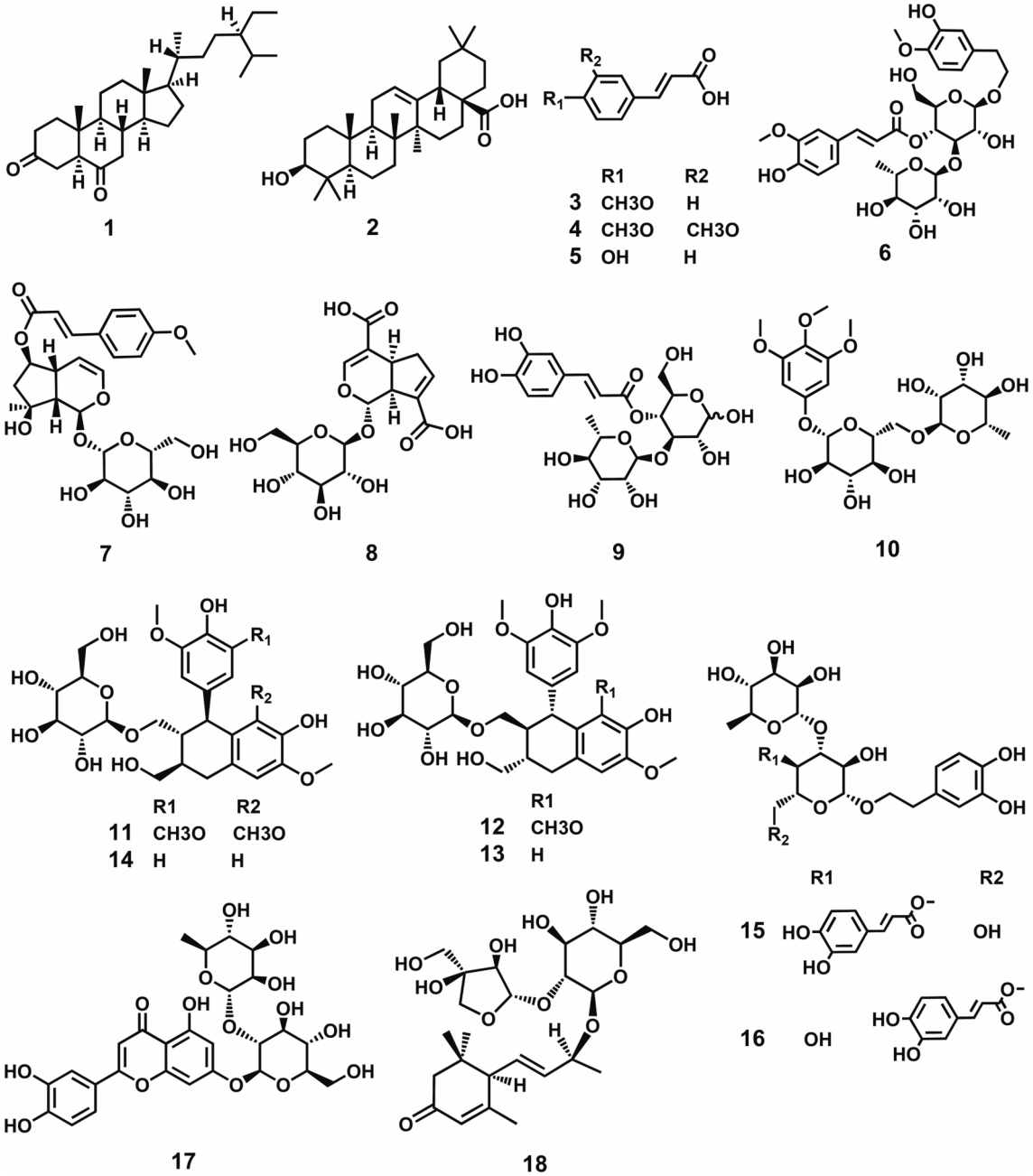

Fig. 2. Structure of compounds (**1–18**) isolated from *D. spathacea*.

m/z 697.2341, $C_{31}H_{40}O_{15}$. ^{1}H NMR (500 MHz, MeOD) δ_H 7.68 (d, J = 15.9 Hz, 1H, H- β'), 7.22 (d, J = 2.0 Hz, 1H, H-2''), 7.10 (dd, J = 8.2, 2.0 Hz, 1H, H-6''), 6.85 (d, J = 5.5 Hz, 1H, H-5''), 6.83 (d, J = 5.4 Hz, 1H, H-5), 6.76 (d, J = 2.2 Hz, 1H, H-2), 6.71 (dt, J = 8.2, 2.6 Hz, 1H, H-6), 6.39 (d, J = 15.9 Hz, 1H, H- α'), 5.22 (d, J = 1.8 Hz, 1H, H-1''), 4.94 (t, J = 9.3 Hz, 1H, H-4'), 4.39 (dd, J = 10.9, 7.9 Hz, 1H, H-1'), 3.91 and 3.83 (each 3H, s, 2 × OMe), 1.12 (d, J = 6.2 Hz, 3H, 3H-6''). ^{13}C NMR (125 MHz, MeOD) δ_C 168.2 (C-CO), 150.9 (C-4''), 149.4 (C-3''), 147.9 (C-β'), 147.6 (C-3), 147.4 (C-4), 132.9 (C-1), 127.6 (C-1''), 124.4 (C-6''), 121.1 (C-6), 117.1 (C-5), 116.5 (C-5''), 115.1 (C-α'), 112.9 (C-2), 111.8 (C-2''), 104.2 (C-1'), 103.0 (C-1''), 81.5 (C-3'), 76.2 (C-2'), 76.1 (C-5'), 73.8 (C-4''), 72.3 (C-2''), 72.1 (C-α), 72.1 (C-3''), 70.6 (C-4'), 70.4 (C-5''), 62.4 (C-6'), 56.5 (C-OMe), 56.4 (C-OMe), 36.6 (C-β), 18.4 (C-6'') (Calis et al., 1984).

6-O-(*p*-methoxy-*E*-cinnamoyl)-ajugol **(7):** white amorphous powder, HRESI-MS $[M + H]^+$ *m/z* 509.2018, $C_{25}H_{32}O_{11}$. ^{1}H NMR (600 MHz, MeOD) δ_H 7.70 (d, J = 16.0 Hz, 1H, H-3''), 7.59 (d, J = 8.7 Hz, 2H, H-5'', H-8''), 7.00 (d, J = 8.8 Hz, 2H, H-6'', H-9''), 6.45 (d, J = 15.9 Hz, 1H, H-2''), 6.26 (dd, J = 6.3, 2.3 Hz, 1H, H-3), 5.54 (d, J = 2.6 Hz, 1H, H-1), 5.02 (dd, J = 6.4, 2.9 Hz, 1H, H-4), 4.98 (ddd, J = 6.7, 4.2, 2.6 Hz, 1H, H-6), 4.71 (d, J = 7.9 Hz, 1H, H-1'), 3.94 (dd, J = 11.9, 2.2 Hz, 1H), 3.87 (s, 3H, 3H-OMe), 3.71 (dd, J = 11.9, 5.9 Hz, 1H, H-6'), 2.97 (dd, J = 9.3, 2.8 Hz, 1H, H-5), 2.62 (dd, J = 9.3, 2.5 Hz, 1H, H-9), 2.29 (dd, J = 14.2, 6.5 Hz, 1H, H-7 β), 2.04 (dd, J = 14.3, 4.1 Hz, 1H, H-7α), 1.43 (s, 3H, 3H-10). ^{13}C NMR (150 MHz, MeOD) δ_C 166.8 (C-1''), 161.1 (C-7''), 144.1 (C-3''), 139.0 (C-3), 128.9 (C-5''), 128.9 (C-9''), 126.3 (C-4''), 114.3 (C-2''), 113.3 (C-6''), 113.3 (C-8''), 102.5 (C-4), 97.3 (C-1'), 91.4 (C-1), 78.3 (C-6), 77.1 (C-8), 76.1 (C-5'), 75.9 (C-3'), 72.7 (C-2'), 69.6 (C-4'), 60.8 (C-6'), 53.8 (C-OMe), 49.6 (C-9), 45.8 (C-7), 37.3 (C-5), 24.0 (C-10) (Nguyen et al., 2018).

Scolymoside **(17):** yellow amorphous powder, HRESI-MS $[M-H]^-$ *m/z* 593.1502, $C_{27}H_{30}O_{15}$. ^{1}H NMR (500 MHz, MeOD) δ_H 7.39 (dq, J = 4.3, 2.2 Hz, 2H, H-2', H-6'), 6.91 (d, J = 8.9 Hz, 1H, H-5'), 6.72 (d, J = 2.2 Hz, 1H, H-8), 6.58 (s, 1H, H-3), 6.50 (d, J = 2.1 Hz, 1H, H-6), 5.03 (d, J = 7.4 Hz, 1H, H-1''), 4.71 (d, J = 1.6 Hz, 1H, H-1''), 4.05 (d, J = 9.5 Hz, 1H, H-6''b), 3.90 (dd, J = 3.5, 1.7 Hz, 1H, H-2''), 1.18 (d, J = 6.2 Hz, 3H, H-6''). ^{13}C NMR (125 MHz, MeOD) δ_C 182.8 (C-4), 165.7 (C-2), 163.5 (C-7), 161.7 (C-5), 157.7 (C-9), 150.0 (C-4'), 145.8 (C-3'), 122.3 (C-1'), 119.4 (C-6'), 115.7 (C-5'), 113.1 (C-2'), 105.9 (C-10), 103.0 (C-3), 100.9 (C-1''), 100.4 (C-1''), 99.9 (C-6), 94.9 (C-8), 76.6 (C-5''), 75.9 (C-3''), 73.5 (C-4''), 72.8 (C-2''), 71.2 (C-2''), 70.9 (C-3''), 70.1 (C-4''), 68.6 (C-5''), 66.3 (C-6''), 16.7 (C-6'') (Guvenalp et al., 2015).

3.3. Evaluation of xanthine oxidase inhibitory activity and kinetics for six highly potential compounds

Eighteen compounds (**1**–**18**) of *D. spathacea* leaves were assessed for XO inhibitory activity, and the assay was based on the oxidation of the substrate xanthine to uric acid in the presence of xanthine oxidase. Only six compounds (**3**–**7** and **17**) exhibited XO inhibitory activity with IC_{50} values ranging from 19.34 ± 1.63 μM to 64.50 ± 0.94 μM compared to the positive control-allopurinol (IC_{50} 2.42 ± 0.30 μM), shown in Table 1.

Table 1
Xanthine oxidase inhibitory activity of bioactive compounds of *D. spathacea*.

Compounds	IC_{50} # (μM)	Type of Inhibition
Trans-4-methoxycinnamic acid **(3)**	26.35 ± 3.36[a]	competitive
Trans-3,4-dimethoxycinnamic acid **(4)**	48.61 ± 6.01[b]	competitive
p-Coumaric acid **(5)**	23.32 ± 1.88[a]	competitive
Martynoside **(6)**	64.50 ± 0.94[c]	mixed
6-*O*-(*p*-methoxy-*E*-cinnamoyl)-ajugol **(7)**	46.73 ± 5.59[b]	competitive
Scolymoside **(17)**	19.34 ± 1.63[a]	competitive
Allopurinol *	2.42 ± 0.30	competitive

Results are expressed as mean ± SD of three independent experiments. #IC_{50}: Half-maximal inhibitory concentration; * as a positive control. If different superscript letters indicate significant differences ($p < 0.05$). If superscripts are the same, there is no significant difference ($p \geq 0.05$).

Lineweaver–Burk double reciprocal plots revealed that compounds **3**, **4**, **5**, **7**, and **17** were competitive xanthine oxidase inhibitors with a mode of action similar to allopurinol. In contrast, compound **6** inhibits xanthine oxidase in a mixed-type manner (Fig. 3). Subsequently, the interaction of the active compounds with the XO enzyme was determined through molecular docking.

3.4. Enzyme interaction pattern of potent XO inhibitory compounds by molecular docking computation

The computational investigate was conducted to understand further the potential molecular interaction patterns between XO enzyme and six identified potency inhibitors (*trans*-4-methoxycinnamic acid **(3),** *trans*-3,4-dimethoxycinnamic acid **(4),** *p*-coumaric acid **(5),** martynoside **(6),** 6-O-(*p*-methoxy-*E*-cinnamoyl)-ajugol **(7),** scolymoside **(17)**). This study employed molecular docking to elucidate the interplay between these molecules and the XO protein. Of specific interest was the elucidation of the structural amino acid residues within the active site cavity, which play a pivotal role in achieving effective and selective inhibition of XO activity.

From the corresponding six molecular docking simulations, the most appropriate docking poses for each compound were selected based on the lowest binding free energy, aiming to elucidate their respective mechanisms of action. The docking conformations for each compound's selected pose were shown in Supplementary data Fig. 55S, while the potential molecular interaction patterns were listed in Table 2.

Notably, the predictive analysis, substantiated by molecular docking, unequivocally confirmed the capacity of all six compounds to inhibit XO enzyme activity. Among these, scolymoside **(17)** emerged as particularly noteworthy, displaying the lowest binding energy of −18.3286 kcal/mol, corresponding to the lowest IC_{50} value, 19.34 ± 1.63 μM. The compounds **3**, **4**, **5**, **6**, and **7** have binding energy values of −15.2052, −12.0238, −16.4156, −5.6664, and −10.2515 kcal/mol, respectively, which are higher compared to allopurinol-positive control, −28.6850 kcal/mol (Table 2). All compounds interacted with key residues by forming hydrogen bonds; compound **17** forms six hydrogen bonds with MoS3004, Arg880, Thr1010, Ala1079, and Glu1261; compound **3** forms two hydrogen bonds with Asn768 and Ser876; compound **4** forms one hydrogen bond with Asn768; compound **5** forms two hydrogen bonds with Lys771 and Ser876; compound **6** forms three hydrogen bonds with Asn650, Lys771, and Thr1010; compound **7** forms two hydrogen bonds with Leu648, and Lys771. Furthermore, compounds **3,** and **17** form pi-pi T-stacked interactions with the amino acid Phe649 through aromatic rings, as shown in Table 2, Fig. 4 and Supplementary data Fig. 55S.

4. Discussion

Gout is a prevalent form of arthritis that stems from a metabolic disorder called hyperuricemia. The disorder is marked by high levels of uric acid in the blood. The body's primary source of uric acid is the breakdown of purine bases. The process begins with the formation of hypoxanthine as a byproduct, which then converts into xanthine. Finally, uric acid is synthesized from xanthine through the enzymatic action of xanthine oxidase (Liu et al., 2021). There is a growing trend in using medicinal plants to develop new pharmaceuticals. This trend is motivated by the goal of creating highly effective medications for treating ailments while minimizing or completely avoiding side effects. The therapeutic properties of these plants are closely associated with the presence of valuable phytochemical compounds like flavonoids, tannins, saponins, and several other beneficial substances (Mehmood et al., 2019).

Various species within the Dolichandrone genus have been studied for their medicinal properties, encompassing many benefits. These properties include anticancer, anti-inflammatory, hepatoprotective, neuroprotective, hypolipidemic, anti-fever, hypoglycemic, antimicrobial, anxiolytic, anti-mutagenic, and antioxidant activities (Badgujar

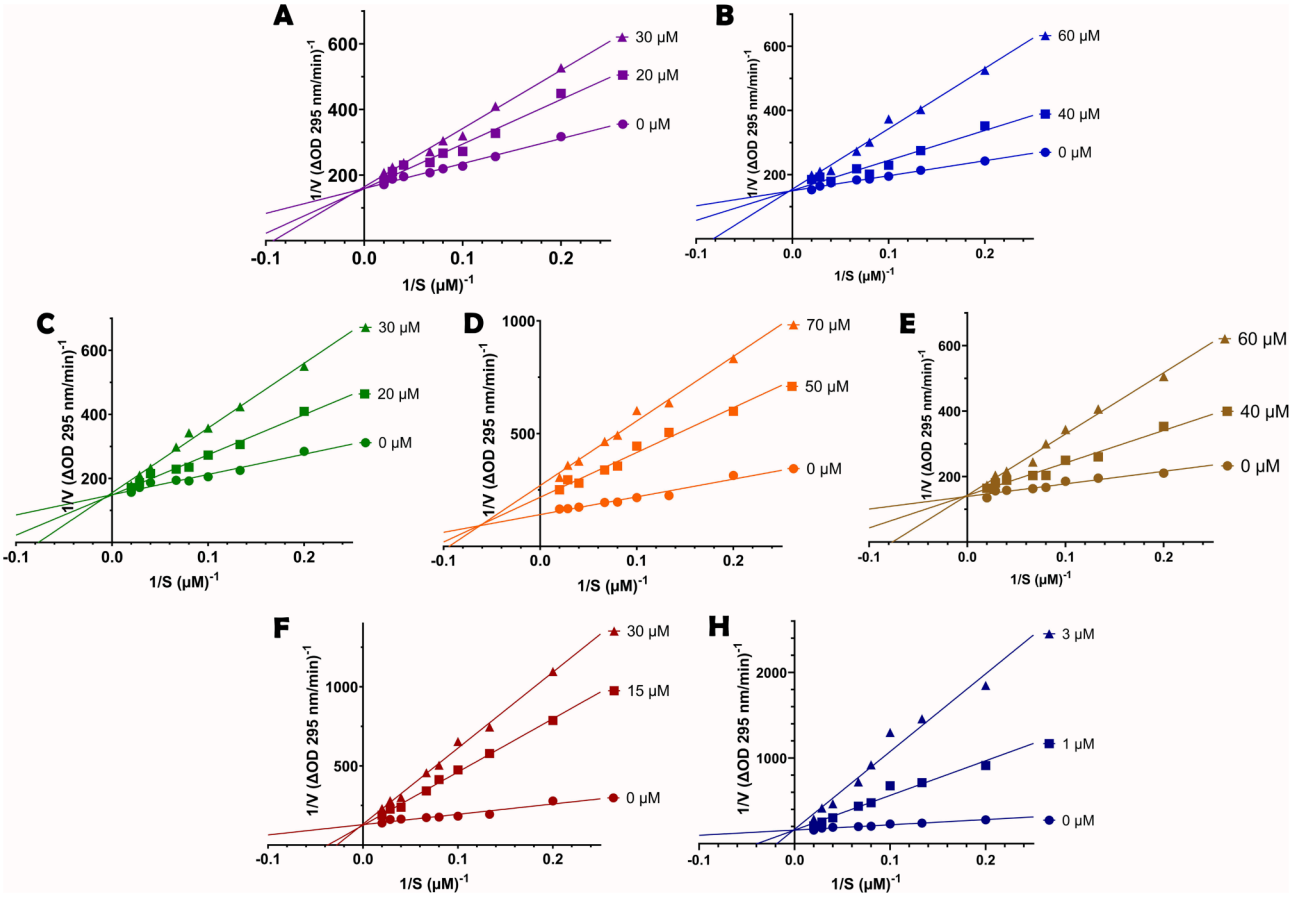

Fig. 3. Lineweaver-Burk plots of inhibition of xanthine oxidase by (A) *trans*-4-methoxycinnamic acid **(3)**; (B) *trans*-3,4-dimethoxycinnamic acid **(4)**; (C) *p*-coumaric acid **(5)**; (D) martynoside **(6)**; (E) 6-*O*-(*p*-methoxy-*E*-cinnamoyl)-ajugol **(7)**; (F) scolymoside **(17)**; (H) Allopurinol. Each point is the average value from three independent experiments.

Table 2
Docking ability and affinity of potential ligands with XO.

Compounds	ΔG (Binding free energy) (kcal/mol)	Interaction residues			
		Hydrogen bonds	pi-Sigma	pi-pi T-stacked	pi-alkyl
Trans-4-methoxycinnamic acid (**3**)	−15.2052	Asn768, Ser876	Val1011	Phe649	Leu648,Leu1014
Trans-3,4-dimethoxycinnamic acid (**4**)	−12.0238	Asn768	Val1011	–	Phe1013, Leu1014
p-Coumaric acid (**5**)	−16.4156	Lys771, Ser876	–	–	Leu873,Val1011, Leu1014
Martynoside (**6**)	−5.6664	Asn650, Lys771, Thr1010	Val1011	–	Phe1013
6-*O*-(*p*-methoxy-*E*-cinnamoyl)-ajugol (**7**)	−10.2515	Leu648, Lys771	–	–	Leu873, Phe914, Val1011, Leu1014, Pro1076
Scolymoside (**17**)	−18.3286	MoS3004, Arg880, Thr1010, Ala1079, Glu1261	Phe914	Phe649	Leu648, Val1011, Phe1009
Allopurinol [#]	−28.6850	MoS3004, Glu802, Arg880, Thr1010, Ala1079	–	–	–

BE, binding free energy; [#], positive control. -, no interaction.

and Surana, 2010, Nguyen et al., 2018, Chaimontri et al., 2021, Yellurkar et al., 2021). The present study is the first to identify and characterize the phytochemical constituents with potential XO inhibition of *D. spathacea*. According to the XO interaction inhibition test results, the crude extract showed medium inhibitory activity compared to the positive control–allopurinol. At a concentration of 100 μg/mL, the crude extract exhibited a significant XO inhibitory activity of 61.43 ± 8.41 %, which corresponds to an IC_{50} of 85.01 μg/ml, is well comparable to a corresponding value for the XO inhibition by the seed extract of *Semecarpus anacardium* (IC_{50}: 253 μg/ml) (Arimboor et al., 2011). Some other plants were investigated XO inhibitory activities, such as *Centaurium erythraea* (IC_{50}: 73.2 μg/ml), *Olea europaea* (IC_{50}: 42 μg/ml) and *Rhus coriaria* (IC_{50}: 172.5 μg/ml) (Valentão et al., 2001, Candan, 2003, Flemmig et al., 2011). This indicates that the crude extract contains compounds with potential XO inhibitory properties (Gainche et al., 2021, Yuk et al., 2023).

When evaluating the XO inhibitory activities among the fractions, the EtOAc fraction displayed the highest, with an inhibition percentage of 78.57 ± 3.85 % at 100 μg/mL, suggesting that this fraction has notable potency in inhibiting XO. The BuOH fraction also exhibited considerable XO inhibitory activity, with an inhibition percentage of 69.43 ± 8.68 % at 100 μg/mL, slightly lower than the EtOAc fraction,

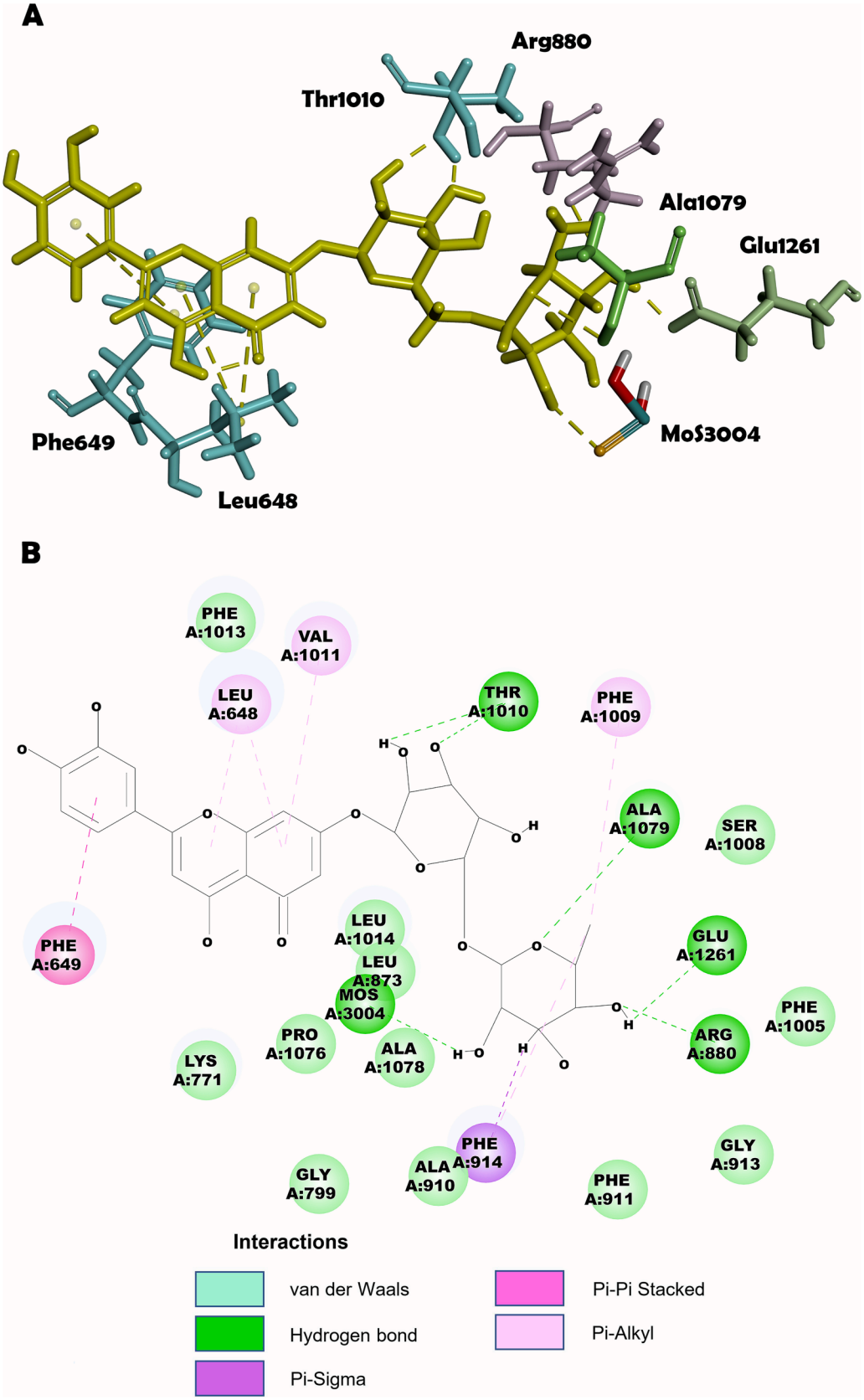

Fig. 4. The interaction mechanism of scolymoside (**17**) with xanthine oxidase (1N5X) was visualized by (A) 3D diagram and (B) 2D diagram.

which also signifies a substantial inhibitory effect, as reported by previous XO inhibitory research (Noor Hashim et al., 2013). Furthermore, the EtOAc and BuOH fractions from *D. spathacea* showed concentration-dependent inhibition of XO, as evidenced by their differing activities at 100 μg/mL and 50 μg/mL, similar to the inhibitory potential against XO depending on the concentration of *Alocasia longiloba*, Urinile (Ahmad et al., 2020, Alam et al., 2021). The hexane fraction displayed the lowest XO inhibitory activity of 27.11 ± 2.50 % at 100 μg/mL among the fractions tested (Supplementary data Table 2S), so this fraction was not subjected to further research. *In vitro* assays demonstrated moderate inhibition of XO by the EtOAc (IC_{50} = 55.93 μg/ml) and BuOH fractions (IC_{50} = 70.17 μM) when compared to allopurinol (IC_{50} = 2.42 μM). The XO inhibitory activities of flavonoids, hydroxycinnamic acids, tannins, and phenylethanoid glycosides have been reported in previous studies (Nagao et al., 1999, Hofmann et al., 2016, Mehmood et al., 2019). It suggests that in EtOAc and BuOH fractions, there is likely the presence of constituents belonging to phenolic, which contributed to XO inhibition. So, these fractions were subsequently subjected to further fractionation and purification to obtain pure compounds. Total 18 compounds were isolated and elucidated, including cyclolignans (compounds **11, 12, 13, 14**), hydroxycinnamic acid derivatives (compounds **3, 4, 5**), phenylpropanoid glycosides (compounds **6, 15, 16**), iridoid glucosides (compounds **7, 8**), phenylethanoid glycosides (compound **9**), phenolic glycosides (compound **10**), flavonoids (compound **17**), steroids (compound **1**), triterpenoids (compound **2**), norisoprenoids (compound **18**). Chemical diversities are pivotal in exploring natural sources for potential therapeutic agents (Clark, 1996).

The study revealed 6 potential constituents (compounds **3**, **4**, **5**, **6**, **7**, **17**) with good XO inhibitory activity from *D. spathacea*. Notably, scolymoside **(17)**, which belongs to flavonoids, exhibited remarkable inhibitory potency with an IC_{50} value of 19.34 ± 1.63 μM. The kinetic data indicated that scolymoside (**17**) acts as a competitive inhibitor of xanthine oxidase, as shown in Fig. 3**F**, as the same type of competitive inhibition was found in the case of flavonoids such as apigenin, quercetin, myricetin, and genistein (Lin et al., 2002). Consequently, it inhibited XO by binding with the free enzyme, forming an enzyme-inhibitor complex. This complex is non-reactive, preventing the enzyme from generating the product. The inhibitor competes directly with the substrate for binding to the enzyme. In typical conditions, the substrate would bind to the active site of the enzyme. Likewise, competitive inhibitors also bind to the enzyme's active site (Ochs et al., 2000). Generally, flavonoids exhibit two primary xanthine oxidase (XO) inhibition modes: competitive and mixed-type. The structural characteristics of flavonoids may play a role in influencing these inhibition modes (Lin et al., 2002, Zhao et al., 2020). Scolymoside **(17)** has two phenyl rings (A and B), a heterocyclic ring (ring C), and hydroxyl groups (C-5 and C-7) on the A ring, possessing strong XO inhibitory activities. It's worth noting that hydroxyl groups on the B ring of flavonoids play a crucial role in their XO inhibitory potential (Hsu et al., 2021), as reported by a previous study (Qu et al., 2017). This finding suggests that scolymoside (**17**) could serve as a promising lead compound for the development of novel xanthine oxidase inhibitors, which (IC_{50} = 19.34 μM) has better inhibitory ability than other compounds also have a similar skeleton structure of flavones, such as 6-hydroxyluteolin-7-O-glycoside, baicalein, and baicalin, which have been reported for their XO inhibitory activity with IC_{50} values of 30.4 μM, 46.2 μM, and 123.0 μM, respectively (Nagao et al., 1999, Cheng et al., 2015). In particular, luteolin, which structurally constitutes the aglycone part of scolymoside (**17**), has been evaluated for its potent XO inhibitory activity, demonstrating an inhibition constant (K_i) of 2.38 μM and an IC_{50} of 4.79 μM. Luteolin reduces XO activity through competitive inhibition (Yan et al., 2013). It suggests that the aglycon of scolymoside (**17**) plays a vital role in XO inhibition. Another flavone derivative similar to scolymoside (**17**), namely luteoloside, also exhibited XO inhibitory activity. The luteoloside–XO interaction was spontaneous, and like the aglycone of scolymoside (**17**)-luteolin, luteoloside induced changes in the secondary structure of XO. It elevated the hydrophobicity of XO by forming hydrogen bonds and hydrophobic forces (Chen et al., 2022). These propose that different moieties of flavones may influence the binding modes and sites with XO, thereby impacting XO activity. In addition to its xanthine oxidase inhibitory activity, scolymoside (**17**) also exhibits anticoagulant and antiplatelet activities, inhibits lipopolysaccharide (LPS)-induced expression, and demonstrates hepatoprotective effects (Lee and Bae, 2015, Yoon et al., 2015, Lee and Bae, 2020).

Compounds **3, 4, 5, 6,** and **7** are derivatives of hydroxycinnamic compounds. Among them, compounds **3, 4,** and **5** are phenylpropanoid derivatives (C6-C3) with IC_{50} values of 26.35 ± 3.36 μM, 48.61 ± 6.01 μM, and 23.32 ± 1.88 μM, respectively, displayed moderate inhibitory activity. Structurally, *p*-coumaric acid (**5**) includes a hydroxyl group on the benzene moiety, making it the most potent inhibitor against xanthine oxidase (XO). *Trans*-4-methoxycinnamic acid (**3**) and *trans*-3,4-dimethoxycinnamic acid (**4**) share a similar structure with p-coumaric acid (**5**), with the distinction being one or two methoxy groups replacing the hydroxyl group. This structural modification reduces the inhibitory potency of compounds (**3**) and (**4**) against XO. In comparing the hydrogen atom of the hydroxyl group with the methyl group, it was found to be essential for binding, as trans p-methoxycinnamic acid (**3**) exhibited significantly lower activity than p-coumaric acid (**5**) in binding to XO. This suggests that the hydrogen atom of the hydroxyl group plays a more crucial role than the methyl group in XO inhibitory activity. Additionally, the structure–activity relationships (SARs) of caffeic acid analogs and hydroxycinnamic acid derivatives interacting with the XO enzyme have been reported in previous studies (Chan et al., 1995, Ngoc et al., 2012, Huang et al., 2018). These emphasize the critical role of the cinnamic acid scaffold in xanthine oxidase inhibition. About kinetic inhibition, compounds **3, 4,** and **5** inhibit XO through a competitive mechanism (Fig. 3A-C), similar inhibition type of caffeic acid (IC_{50} = 85.4 μM) and methyl caffeate (IC_{50} = 12.3 μM), which are also phenylpropanoid derivatives (C6-C3) (Nguyen et al., 2006). Compound 6 is a phenylpropanoid glycoside, exhibiting xanthine oxidase inhibitory activity with an IC_{50} value of 64.50 ± 0.94 μM. Similar to angoroside C and incanoside D, which are also phenylpropanoid glycosides, being moderate inhibitors of the xanthine oxidase enzyme (Mostafa et al., 2007). Compound **6** belongs to the mixed-type competitive manner, bind to either the free xanthine oxidase or the XO-substrate complex. The data line of compound **6** intersected within the second quadrant. As the inhibitor concentrations increased, both the intercept values on the horizontal axis ($-1/K_m$) and the vertical axis ($1/V_{max}$) also increased (Fig. 3D). Compound **7** is an iridoid glycoside with a phenylpropanoid skeleton, having an IC_{50} value of 46.73 ± 5.59 μM, belonging to competitive inhibition (Fig. 3E). Martynoside **(6)** and 6-O-(p-methoxy-E-cinnamoyl)-ajugol **(7)** both belong to the class of glycosides and exhibited moderate inhibitory activity. It suggests that the presence of glycosidic moieties may influence the inhibitory potential of these compounds. Further structural modifications and investigations into the glycosidic components may lead to the development of more potent xanthine oxidase inhibitors (Kong et al., 2001, Ye et al., 2020). The XO inhibitory activities of compounds **4** and **7** were reported for the first time, contributing to the potential of natural products for treating hyperuricemia.

To gain deeper insights into the binding interactions between the isolated compounds and xanthine oxidase, in silico molecular docking studies were conducted. The computational analysis provided a molecular basis for the observed inhibitory activity, elucidating the key interactions between the compounds and the enzyme's active site (Śledź and Caflisch, 2018). The XO inhibitory activity of flavonoids has been reported to be attributed to high affinity to some amino acid residues present in the cavity of the narrow channel leading from the active site to the molybdenum center of the catalytic site, hydrogen bonds, which were crucial in stabilizing the complex between the ligands and targets, pi-pi T-stacked interactions are essential for the organization of biomolecular structures (Brylinski, 2018, Bitencourt-Ferreira et al., 2019,

Hsu et al., 2021). The research conducted by Ribeiro et al. regarding the catalytic mechanism of XO revealed that the enzyme facilitates the conversion of xanthine into uric acid in the presence of a molybdenum cofactor. The mechanism involves four reaction steps. In the second step, a hydride is transferred from the tetrahedral intermediate to the sulfur atom of the molybdenum cofactor, which reduces Mo(VI) to Mo(IV). For xanthine oxidase (XO) to facilitate the oxidation process, the substrate must bind to the molybdenum center. Once this binding occurs, electrons are introduced at the molybdenum site; these electrons are then subsequently shuttled to the FAD cofactor (Bachmann, 2009); when inhibitors interact with the molybdenum cofactor, they disrupt and hinder this entire process. In the third step, Arg880 protonates one molecule of uric acid. The research also highlights the crucial role of Arg880 in the catalytic mechanism and the significance of Glu802 in substrate binding. Glu802 stabilizes the negative charge generated in the transition state structure of xanthine, making it essential to the reaction. The research showed that the molybdenum cofactor, Arg880, and Glu802 were the key elements that play essential roles in the catalytic mechanism of XO (Ribeiro et al., 2020). Compounds **4, 5, 6**, and **7** do not engage with the critical elements in the binding site, whereas compound **3** forms a single interaction with Glu802 (Supplementary data Fig. 55S). This specific interaction with Glu802 is a significant factor in explaining the lower binding energy and exerts a more potent XO inhibitory activity of compound **3** than the above compounds. Especially, compound **17** creates interactions with MoS3004 and Arg880, similar to the positive control, allopurinol: MoS3004, Glu802, and Arg880 **(**Fig. 4**)**. When scolymoside **(17)** was placed in XO's active site, the 3′-hydroxyphenyl group of the glucoside part interacted with the molybdenum domain, which plays a vital role in the catalytic mechanism of XO enzyme. In addition, scolymoside **(17)** had one Pi-sigma interaction between the glucoside with Phe914. The aglycone of scolymoside **(17)**, luteolin, was found to be inserted into the hydrophobic region of XO, interacting with Leu873, Leu1014, and Val1011. These hydrophobic interactions were found to potentially contribute to the more significant inhibitory activity of scolymoside (**17**) against XO (Tung et al., 2010). All of these contribute to explaining the lowest IC_{50} value (19.34 ± 1.63 μM) and the lowest binding energy (−18.3286 kcal/mol) of scolymoside (**17**) compared to the other five XO inhibitors studied, as shown in Table 2 and Fig. 4.

Based on the bioactivity and docking results, the six isolated compounds (**3**–**7** and **17**) have the potential to inhibit xanthine oxidase, considered active main constituents of *D. spathacea* for treating hyperuricemia disease by preventing the production of uric acid.

5. Conclusion

In this study, the EtOAc and BuOH fractions and isolated compounds demonstrated the xanthine oxidase inhibitory activities, being investigated for the first time of *D. spathacea* leaves. Eighteen known compounds were successfully isolated and elucidated from this species; nine were previously unreported, and nine were reported. Six of these compounds exhibited potential as xanthine oxidase inhibitors, either through a competitive or mixed-type mechanism, with IC_{50} values ranging from 19.34 ± 1.63 μM to 64.50 ± 0.94 μM. Docking studies were carried out to understand the molecular interactions between xanthine oxidase and the XO-inhibited compounds, and scolymoside **(17)** was found to exhibit the lowest binding energy (−18.3286 kcal/mol), which corresponds to the lowest IC_{50} value (19.34 ± 1.63 μM). These findings suggest that the *D. spathacea* plant has promising potential in the treatment of gout.

Funding

This work was supported by the Ministry of Science and Technology of the Republic of China (Taiwan) [grant number MOST 110-2320-B-038-039 -MY3].

Declaration of competing interest

The authors declare that they have no known competing financial interests or personal relationships that could have appeared to influence the work reported in this paper.

Acknowledgments

We are grateful to Dr. Shwu-Huey Wang and Miss Chia-Wei Ku for the NMR data acquisition by the TMU Core Facility.

Appendix A. Supplementary material

Supplementary data to this article can be found online at https://doi.org/10.1016/j.jsps.2024.101980.

References

Abdulhafiz, F., Mohammed, A., Kayat, F., et al., 2020. Xanthine oxidase inhibitory activity, chemical composition, antioxidant properties and GC-MS analysis of Keladi Candik (Alocasia longiloba Miq). Molecules. 25 https://doi.org/10.3390/molecules25112658.

Ahmad, S., Mohiuddin, E., Shah, S.M.A., et al., 2020. Therapeutic efficacy of urinile against gouty arthritis. Dose Response. 18 https://doi.org/10.1177/1559325820946934.

Alam, M., Uddin, G., Rashid, U., et al., 2021. In vitro and in silico xanthine oxidase inhibitory potential of Benzofuran isolated from *Viburnum grandiflorum* Wall. Ex DC. S. Afr. J. Bot. 143, 359–362. https://doi.org/10.1016/j.sajb.2021.01.010.

Andrianaivoravelona, J.O., Terreaux, C., Sahpaz, S., et al., 1999. A phenolic glycoside and N-(p-coumaroyl)-tryptamine from Ravensara anisata. Phytochemistry. 52, 1145–1148. https://doi.org/10.1016/S0031-9422(99)00377-5.

Arimboor, R., Rangan, M., Aravind, S.G., et al., 2011. Tetrahydroamentoflavone (THA) from Semecarpus anacardium as a potent inhibitor of xanthine oxidase. J. Ethnopharmacol. 133, 1117–1120. https://doi.org/10.1016/j.jep.2010.10.027.

Arshad, M.A., Ahmad, S., Khurshid, U., et al., 2018. Studies on the antioxidant and xanthine oxidase inhibition potential of *Heliotropium crispum*. Acta Pol. Pharm. 75, 41–44.

Bachmann, K., 2009. Chapter 8 - drug metabolism. In: Hacker, M., Messer, W., Bachmann, K. (Eds.), Pharmacology. Academic Press, San Diego, pp. 131–173.

Badgujar, V., Surana, S., 2010. Anxiolytic effects of *Dolichandrone falcata* Seem., Bignoniaceae, stem-bark in elevated plus maze and marble burying test on mice. Rev. Bras. Farmacogn. 20, 773–780. https://doi.org/10.1590/S0102-695X2010005000028.

Bitencourt-Ferreira, G., Veit-Acosta, M., de Azevedo Jr., W.F., 2019. Hydrogen bonds in protein-ligand complexes. Methods Mol. Biol. 2053, 93–107. https://doi.org/10.1007/978-1-4939-9752-7_7.

Brylinski, M., 2018. Aromatic interactions at the ligand-protein interface: Implications for the development of docking scoring functions. Chem. Biol. Drug Des. 91, 380–390. https://doi.org/10.1111/cbdd.13084.

Bylka, W., 2004. *E*- and *Z*-*p*-methoxycinnamic acid from *Aquilegia vulgaris*. Acta Pol. Pharm. 61, 307–308.

Calis, I., Lahloub, M.F., Rogenmoser, E., et al., 1984. Isomartynoside, a phenylpropanoid glycoside from *Galeopsis pubescens*. Phytochemistry. 23, 2313–2315. https://doi.org/10.1016/S0031-9422(00)80542-7.

Candan, F., 2003. Effect of Rhus coriaria L. (Anacardiaceae) on superoxide radical scavenging and xanthine oxidase activity. J. Enzyme Inhib. Med. Chem. 18, 59–62. https://doi.org/10.1080/1475636031000069273.

Chaimontri, C., Arun, S., Sawatpanich, T., et al., 2021. The effect of Dolichandrone serrulata (wall. ex DC.) Seem. flower extract containing antioxidant capacity and terpenoids on the male reproductive system. Andrologia. 53, e13966.

Chan, W.S., Wen, P.C., Chiang, H.C., 1995. Structure-activity relationship of caffeic acid analogues on xanthine oxidase inhibition. Anticancer Res. 15, 703–707.

Chen, J., Wang, Y., Pan, X., et al., 2022. Study on the interaction mechanism between luteoloside and xanthine oxidase by multi-spectroscopic and molecular docking methods. J. Mol. Recogn. 35, e2985.

Cheng, L.C., Murugaiyah, V., Chan, K.L., 2015. In vitro Xanthine oxidase inhibitory studies of *Lippia nodiflora* and isolated flavonoids and phenylethanoid glycosides as potential uric acid-lowering agents. Nat Prod Commun. 10, 945–948.

Choudhary, D.K., Mishra, A., 2019. In vitro and in silico interaction of faba bean (Vicia faba L.) seed extract with xanthine oxidase and evaluation of antioxidant activity as a therapeutic potential. Nat. Prod. Res. 33, 2689–2693. https://doi.org/10.1080/14786419.2018.1460831.

Clark, A.M., 1996. Natural products as a resource for new drugs. Pharm. Res. 13, 1133–1141. https://doi.org/10.1023/A:1016091631721.

de Santana Aquino, D.F., Signor Tirloni, C.A., Tolouei Menegati, S.E.L., et al., 2017. Alibertia edulis (L.C. Rich.) A.C. Rich – a potent diuretic arising from Brazilian indigenous species. J. Ethnopharmacol. 196, 193–200. https://doi.org/10.1016/j.jep.2016.12.024.

Flemmig, J., Kuchta, K., Arnhold, J., et al., 2011. Olea europaea leaf (Ph.Eur.) extract as well as several of its isolated phenolics inhibit the gout-related enzyme xanthine

oxidase. Phytomedicine. 18, 561–566. https://doi.org/10.1016/j.phymed.2010.10.021.
Gainche, M., Ogeron, C., Ripoche, I., et al., 2021. Xanthine oxidase inhibitors from *Filipendula ulmaria* (L.) maxim. and their efficient detections by HPTLC and HPLC analyses. Molecules. 26 https://doi.org/10.3390/molecules26071939.
Guvenalp, Z., Ozbek, H., Karadayi, M., et al., 2015. Two antigenotoxic chalcone glycosides from *Mentha longifolia* subsp. longifolia. Pharm. Biol. 53, 888–896. https://doi.org/10.3109/13880209.2014.948633.
Hofmann, E., Webster, J., Do, T., et al., 2016. Hydroxylated chalcones with dual properties: Xanthine oxidase inhibitors and radical scavengers. Bioorg. Med. Chem. 24, 578–587. https://doi.org/10.1016/j.bmc.2015.12.024.
Hsu, S.-J., Verpoorte, R., Lin, S.-M., et al., 2021. Fast dereplication of xanthine oxidase-inhibiting compounds in alfalfa using comparative metabolomics. Food Res. Int. 141, 110170 https://doi.org/10.1016/j.foodres.2021.110170.
Huang, C.Y., Yeh, T.F., Hsu, F.L., et al., 2018. Xanthine oxidase inhibitory activity and thermostability of cinnamaldehyde-chemotype leaf oil of *Cinnamomum osmophloeum* microencapsulated with β-cyclodextrin. Molecules. 23 https://doi.org/10.3390/molecules23051107.
Ibrahim Dirar, A., Wada, M., Watanabe, T., et al., 2019. Phenolic compounds from the aerial parts of *Blepharis linariifolia* Pers. and their free radical scavenging and enzyme inhibitory activities. Medicines. 6, 113. https://doi.org/10.3390/medicines6040113.
Jackes, B.R., 2017. A revision of Dolichandrone (Bignoniaceae) in Australia. Aust. Syst. Bot. 30, 26–37. https://doi.org/10.1071/SB16031.
Kaewpiboon, C., Lirdprapamongkol, K., Srisomsap, C., et al., 2012. Studies of the in vitro cytotoxic, antioxidant, lipase inhibitory and antimicrobial activities of selected Thai medicinal plants. BMC Compl. Altern. Med. 12, 1–8. https://doi.org/10.1186/1472-6882-12-217.
Kim, J.-K., Si, C.-L., Bae, Y.-S., 2007. Epimeric phenylpropanoid glycosides from inner bark of *Paulownia coreana* Uyeki. Holzforschung. 61, 161–164. https://doi.org/10.1515/HF.2007.029.
Kong, L.D., Abliz, Z., Zhou, C.X., et al., 2001. Glycosides and xanthine oxidase inhibitors from *Conyza bonariensis*. Phytochemistry. 58, 645–651. https://doi.org/10.1016/s0031-9422(01)00176-5.
Lee, I.-C., Bae, J.-S., 2015. Inhibitory effect of vicenin-2 and scolymoside on secretory group IIA phospholipase A2. Anim. Cells Syst. 19, 305–311. https://doi.org/10.1080/19768354.2015.1087428.
Lee, I.-C., Bae, J.-S., 2020. Hepatoprotective effects of vicenin-2 and scolymoside through the modulation of inflammatory pathways. J. Nat. Med. 74, 90–97. https://doi.org/10.1007/s11418-019-01348-x.
Lee, M., Feig, M., Salsbury, F., et al., 2003. New analytic approximation to the standard molecular volume definition and its application to generalized Born calculations. J. Comput. Chem. 24, 1348–1356. https://doi.org/10.1002/jcc.10272.
Lin, C.M., Chen, C.S., Chen, C.T., et al., 2002. Molecular modeling of flavonoids that inhibits xanthine oxidase. Biochem. Biophys. Res. Commun. 294, 167–172. https://doi.org/10.1016/s0006-291x(02)00442-4.
Liu, N., Xu, H., Sun, Q., et al., 2021. The role of oxidative stress in hyperuricemia and xanthine Oxidoreductase (XOR) inhibitors. Oxid. Med. Cell Longev. 2021, 1470380. https://doi.org/10.1155/2021/1470380.
Mehmood, A., Ishaq, M., Zhao, L., et al., 2019. Natural compounds with xanthine oxidase inhibitory activity: a review. Chem. Biol. Drug Des. 93, 387–418. https://doi.org/10.1111/cbdd.13437.
Mostafa, M., Nahar, N., Mosihuzzaman, M., et al., 2007. Free radical scavenging phenylethanoid glycosides from *Leucas indica* Linn. Nat. Prod. Res. 21, 354–361. https://doi.org/10.1080/14786410701194401.
Nagao, A., Seki, M., Kobayashi, H., 1999. Inhibition of xanthine oxidase by flavonoids. Biosci. Biotechnol. Biochem. 63, 1787–1790. https://doi.org/10.1271/bbb.63.1787.
Ngoc, T.M., Khoi, N.M., Ha, D.T., et al., 2012. Xanthine oxidase inhibitory activity of constituents of *Cinnamomum cassia* twigs. Bioorg. Med. Chem. Lett. 22, 4625–4628. https://doi.org/10.1016/j.bmcl.2012.05.051.
Nguyen, P.D., Abedini, A., Gangloff, S., et al., 2016. Phytochemical analysis and antimicrobial evaluation of Dolichandrone spathacea (Bignoniaceae). Planta Med. 81, S1–S381. https://doi.org/10.1055/s-0036-1596346.
Nguyen, P.-D., Abedini, A., Gangloff, S.C., et al., 2018. Antimicrobial constituents from leaves of *Dolichandrone spathacea* and their relevance to traditional use. Planta Med. Int. Open. 5, e14–e23. https://doi.org/10.1055/s-0043-125339.
Nguyen, M.T.T., Awale, S., Tezuka, Y., et al., 2006. Xanthine oxidase inhibitors from the flowers of *Chrysanthemum sinense*. Planta Med. 72, 46–51. https://doi.org/10.1055/s-2005-873181.
Noor Hashim, N.H., Abas, F., Shaari, K., et al., 2013. Antioxidant and xanthine oxidase inhibitory activities of *Persicaria hydropiper*. Int. J. Food Prop. 16, 1028–1036. https://doi.org/10.1080/10942912.2011.575497.
Ochs, R.S., Chem, J., 2000. Educ. J. Chem. Educ. 77, 1453. https://doi.org/10.1021/ed077p1453.
Onoja, E., Ndukwe, I.G., 2013. Isolation of oleanolic acid from chloroform extract of Borreria stachydea[(DC) Hutch. and Dalziel]. J. Nat. Prod. Plant Resour. 3, 57–60.
Paul, B.J., James, R., 2017. Gout: an Asia-Pacific update. Int. J. Rheum. Dis. 20, 407–416. https://doi.org/10.1111/1756-185X.13103.
Pinzi, L., Rastelli, G., 2019. Molecular docking: shifting paradigms in drug discovery. Int. J. Mol. Sci. 20 https://doi.org/10.3390/ijms20184331.
Qu, L., Ruan, J.-Y., Jin, L.-J., et al., 2017. Xanthine oxidase inhibitory effects of the constituents of *Chrysanthemum morifolium* stems. Phytochem. Lett. 19, 39–45. https://doi.org/10.1016/j.phytol.2016.11.007.
Ralph, S., Landucci, L., Ralph, J., 2004. NMR Database of Lignin and Cell Wall Model Compounds, Great lakes bioenergy research center.
Rho, T., Yoon, K., 2017. Chemical constituents of *Nelumbo nucifera* seeds. Nat. Prod. Sci. 23, 253. https://doi.org/10.20307/nps.2017.23.4.253.
Ribeiro, P., Fernandes, H., Maia, L., et al., 2020. The complete catalytic mechanism of xanthine oxidase: a computational study. Inorg. Chem. Front. 8 https://doi.org/10.1039/D0QI01029D.
Saiful, A., Mohtar, M., Mazurah, M., et al., 2011. Inhibitory potential against Methicillin-Resistant Staphylococcus aureus (MRSA) of dolichandrone spathacea, a mangrove tree species of Malaysia. Lat. Am. J. Pharm. 30, 359–362.
Santos, L.H.S., Ferreira, R.S., Caffarena, E.R., 2019. Integrating molecular docking and molecular dynamics simulations. Methods Mol. Biol. 2053, 13–34. https://doi.org/10.1007/978-1-4939-9752-7_2.
Śledź, P., Caflisch, A., 2018. Protein structure-based drug design: from docking to molecular dynamics. Curr. Opin. Struct. Biol. 48, 93–102. https://doi.org/10.1016/j.sbi.2017.10.010.
Suo, M., Ohta, T., Takano, F., et al., 2013. Bioactive Phenylpropanoid Glycosides from *Tabebuia avellanedae*. Molecules. 18, 7336–7345. https://doi.org/10.3390/molecules18077336.
Takeda, Y., Zhang, H., Matsumoto, T., et al., 1997. Megastigmane glycosides from *Salvia nemorosa*. Phytochemistry. 44, 117–120. https://doi.org/10.1016/S0031-9422(96)00359-7.
Thao, T.T.P., Chi, N.L., Luu, N.T., et al., 2021. Phytochemistry and anti-inflammatory activity of iridoids from *Dolichandrone spathacea* collected in the mangrove forest of Phu Loc district, Thua Thien Hue province, VietNam. Vietnam J. Chem. 59, 943–950. https://doi.org/10.1002/vjch.202100121.
Tung, Y.-T., Hsu, C.-A., Chen, C.-S., et al., 2010. Phytochemicals from *Acacia confusa* heartwood extracts reduce serum uric acid levels in oxonate-induced mice: their potential use as xanthine oxidase inhibitors. J. Agric. Food Chem. 58, 9936–9941. https://doi.org/10.1021/jf102689k.
Valentão, P., Fernandes, E., Carvalho, F., et al., 2001. Antioxidant activity of *Centaurium erythraea* infusion evidenced by its superoxide radical scavenging and xanthine oxidase inhibitory activity. J. Agric. Food Chem. 49, 3476–3479. https://doi.org/10.1021/jf001145s.
Van Tuan, N., Do, L.Q., Nguyen, T.A., et al., 2018. New cycloartanes and new iridoids from D*olichandrone spathacea* collected in the mangrove forest of Soc Trang province, VietNam. J. Asian Nat. Prod. Res. 20, 889–896. https://doi.org/10.1080/10286020.2017.1406927.
Wen, Q., Lin, X., Liu, Y., et al., 2012. Phenolic and lignan glycosides from the butanol extract of *Averrhoa carambola* L. Root. Mole. 17, 12330–12340. https://doi.org/10.3390/molecules171012330.
Yan, J., Zhang, G., Hu, Y., et al., 2013. Effect of luteolin on xanthine oxidase: Inhibition kinetics and interaction mechanism merging with docking simulation. Food Chem. 141, 3766–3773. https://doi.org/10.1016/j.foodchem.2013.06.092.
Ye, Z.J., He, X.A., Wu, J.P., et al., 2020. New prenylflavonol glycosides with xanthine oxidase inhibitory activity from the leaves of *Cyclocarya paliurus*. Bioorg Chem. 101, 104018 https://doi.org/10.1016/j.bioorg.2020.104018.
Yellurkar, M.L., Singh, V., Sai Prasanna, V., et al., 2021. Evaluation of a natural compound extracted from *Dolichandrone atrovirens* as a novel antioxidant agent using Caenorhabditis elegans. PLoS One. 16, e0257702.
Yoon, E.K., Ku, S.K., Lee, W., et al., 2015. Antitcoagulant and antiplatelet activities of scolymoside. BMB Rep. 48, 577–582. https://doi.org/10.5483/bmbrep.2015.48.10.044.
Yuk, H.J., Ryu, H.W., Kim, D.S., 2023. Potent xanthine oxidase inhibitory activity of constituents of Agastache rugosa (Fisch. and C.A.Mey.) Kuntze. Foods. 12 https://doi.org/10.3390/foods12030573.
Zhao, J., Huang, L., Sun, C., et al., 2020. Studies on the structure-activity relationship and interaction mechanism of flavonoids and xanthine oxidase through enzyme kinetics, spectroscopy methods and molecular simulations. Food Chem. 323, 126807. https://doi.org/10.1016/j.foodchem.2020.126807.
Zhao, C.-C., Shao, J.-H., Li, X., et al., 2005. Antimicrobial constituents from fruits of *Ailanthus altissima* SWINGLE. Arch. Pharm. Res. 28, 1147–1151. https://doi.org/10.1007/BF02972977.